IOPscience iopscience.iop.org

Home Search Collections Journals About Contact us My IOPscience

Monte Carlo methods for phase equilibria of fluids

This article has been downloaded from IOPscience. Please scroll down to see the full text article.

2000 J. Phys.: Condens. Matter 12 R25

(http://iopscience.iop.org/0953-8984/12/3/201)

View the table of contents for this issue, or go to the journal homepage for more

Download details:
IP Address: 171.66.16.218
The article was downloaded on 15/05/2010 at 19:29

Please note that terms and conditions apply.

J. Phys.: Condens. Matter **12** (2000) R25–R52. Printed in the UK PII: S0953-8984(00)98242-0

REVIEW ARTICLE

Monte Carlo methods for phase equilibria of fluids

Athanassios Z Panagiotopoulos

Institute for Physical Science and Technology and Department of Chemical Engineering, University of Maryland, College Park, MD 20742-2431, USA

E-mail: thanos@ipst.umd.edu

Received 9 October 1998

Abstract. This article presents an overview of Monte Carlo methods for simulations of the phase behaviour of fluids. The Gibbs ensemble method and histogram-reweighting Monte Carlo techniques are described in detail. The Gibbs ensemble method is based on simulations of two regions coupled via volume change and particle transfer moves so that the conditions for phase coexistence are satisfied in a statistical sense. Histogram-reweighting methods obtain the free energy of a system over a broad range of conditions from a small set of grand canonical Monte Carlo calculations. The histogram methods can produce highly accurate data, especially in the vicinity of critical points. Other methods described briefly include interfacial simulations, the NPT + test particle method, Gibbs–Duhem integration and pseudo-ensembles. Configurational-bias sampling techniques and expanded ensembles can be used for multisegment molecules to increase the efficiency of the simulations. The last section of the review covers applications to both model and realistic systems that have appeared since 1995.

1. Introduction

The phase behaviour of fluids and their mixtures is of central importance to many technological and scientific fields, for example in designing separations for the chemical and pharmaceutical industries, understanding fundamental processes in living systems, or even modelling of the global climate. A large body of experimental information has been gathered over the years (e.g. see [1]), and significant efforts have been made to understand the phenomenology of the transitions and obtain empirically and theoretically based models that can be used to correlate and extend the range of experimental data. Experimental measurements are time consuming and expensive. For multicomponent mixtures, measurements are available only for a limited number of temperatures, pressures and compositions. Empirical models are only valid over the range of conditions for which experimental data have been used for obtaining the model parameters. Even theoretically based models have limited predictive abilities for conditions and systems different from the ones for which they have been tested against experimental data [2].

Molecule-based simulations are an increasingly important alternative to experimental measurements and theoretical techniques for obtaining properties of fluids and materials. The focus of the present review is on simulations of phase equilibrium properties of classical fluids. Classical force-field-based simulations start by postulating a functional form for the intermolecular forces in a system. Equilibrium properties can generally be obtained by either Monte Carlo or molecular dynamics methods. Monte Carlo methods are based on generating configurations from the appropriate probability distribution for a statistical

0953-8984/00/030025+28$30.00 © 2000 IOP Publishing Ltd

mechanical ensemble, while molecular dynamics methods generate configurations by solving Newton's equations of motion. Calculations by simulation of simple structural and energetic properties (such as pair correlation functions, the mean configurational energy or pressure) are relatively straightforward, but the prediction of the order and precise location of phase transitions is not a simple matter. Phase transitions are collective phenomena that occur over timescales and length scales that are not directly accessible to molecular dynamics or simple constant-volume Monte Carlo simulations. Until the mid-1980s, obtaining the phase behaviour of even a simple one-component system required a major research effort [3]. Methodological developments since then have rendered the determination of phase equilibria by simulation much easier than before. Most of these methodological advances have involved the development of novel Monte Carlo algorithms, which are the focus of the present review. In addition, the sustained increases in computing hardware capabilities have greatly expanded the range of systems that can be studied on readily available machines. As a result, the number of simulation studies of both model potentials and realistic systems has dramatically increased.

A number of textbooks, research monographs and review articles have appeared previously in the area of the present article. The book by Allen and Tildesley [4] on computer simulation methods for liquids provides an excellent introduction to molecular dynamics and Monte Carlo methods, but does not cover the major recent methodological advances, since it was published in 1987. The recent book by Frenkel and Smit [5] has comprehensive coverage of molecular simulation methods for fluids, with particular emphasis on algorithms for phase equilibrium calculations. It describes many of the techniques mentioned in the present article in significantly more detail than is possible here. The Gibbs ensemble method and its applications have been reviewed in [6–9]. Proceedings of a recent NATO Advanced Study Institute on simulations of phase transitions [10] and general review articles on simulation methods and their applications (e.g. [11–13]) are also available.

Knowledge of the chemical potential of all components (or the free energy) of a system as a function of temperature, density and composition is, of course, sufficient to determine the phase behaviour. Such methods include thermodynamic integration, a very general technique in which the state of interest is linked via a reversible path to a state of known free energy [5], and the Widom test particle insertion method [14]. The present article focuses on methods that were specifically designed for phase equilibrium calculations. The relative precision and accuracy of methods for obtaining the chemical potential have been examined in [15].

The plan of this article is as follows. Direct interfacial simulation methods are reviewed in section 2. Such simulations provide information on the properties of interfaces which cannot be obtained from other techniques, but require relatively large systems and do not give reliable results near critical points. Section 3 deals with the Gibbs ensemble Monte Carlo method, which is based on simultaneous calculations in two regions representing equilibrium phases, coupled indirectly via particle transfers and volume changes. The method is now commonly used for obtaining phase equilibria of fluids, because of its simplicity and speed. A single Gibbs ensemble simulation gives a point on the phase envelope of a multicomponent system. A number of other methods designed for direct calculations of phase equilibria are described in section 4. The NPT + test particle method (section 4.1) is based on chemical potential calculations. The method has roughly the same range of applicability and limitations as the Gibbs ensemble method, but requires multiple simulations per coexistence point. Gibbs–Duhem integration (section 4.2) does not require particle insertions and removals and is applicable for transitions involving solids. It needs to start, however, from a point on the phase envelope determined by one of the other techniques. Pseudo-ensembles (section 4.3)

provide significant flexibility in determinations of phase equilibria under different external constraints and can be implemented in combination with the Gibbs ensemble or Gibbs–Duhem integrations. Histogram-reweighting methods (section 5) provide the free energy and phase behaviour with excellent accuracy and can be used in the vicinity of critical points. The majority of simulation methods for calculations of phase transitions rely on particle transfers, which become impractical for dense systems or multisegment molecules. A number of methods have been developed for improving the efficiency of particle transfers and have been instrumental in enabling calculations for realistic potential models. Configurational-bias sampling techniques that perform 'smart' insertions at favourable locations are described in section 6.1. Expanded ensembles are based on gradual transfers of parts of molecules and are described in section 6.2. The last part of this review (section 7) describes applications of simulations to calculations of the phase behaviour of both highly idealized and realistic intermolecular potential models. The paper concludes with a discussion of the relative strengths and weaknesses of the methods discussed and provides some suggestions for possible future research directions in the field.

2. Direct interfacial simulations

Conceptually, the simplest possible approach for determining phase equilibria by simulation is to set up a system with an explicit interface. Applications of direct interfacial simulations, which can be performed by either Monte Carlo or molecular dynamics algorithms, have been reviewed by Rowlinson and Widom [16] and Gubbins [17]. Despite the simplicity of the approach, there are difficulties associated with setting up and equilibrating a system with two coexisting phases. Simulations involving many particles and long equilibration times are often required even for simple spherically symmetric potentials [18]. Even with large systems, a significant fraction of particles are near the interface and have properties which may not be representative of their behaviour in the bulk. When the density difference between the two coexisting phases is small, it is impossible to set up a stable two-phase system. For fluids with low vapour pressures, for any reasonable system size, very few particles can be found in the gas phase. Direct interfacial simulations do not require particle transfers at random locations, contrary to many other methods described in this review. For dense systems for which such transfers have low acceptance probabilities, direct interfacial methods would seem to have an advantage. However, equilibration of the chemical potential by diffusion through the interface is also exceedingly slow under such conditions [19].

Two-phase simulations have been used when no other practical alternative could be found for the system and conditions of interest [20–22]. An example of a direct interfacial simulation of a model lattice surfactant system is shown in figure 1. The two coexisting phases are a low-density gas phase at the two sides of the simulation cell, and a high-density lamellar phase in the middle. Density modulations within the lamellar phase are evident. One advantage of direct interfacial simulations is that they provide information on the structure of the interface and on the surface tension between coexisting phases [23–27].

An interesting extension of direct interfacial simulation methods is to combine them with configurational-bias concepts described in section 6.1. Such a combination has been described by Yan *et al* [19] for simulations of lattice homopolymers. Configurational-bias moves attempt to take a particle to a new random location in the simulation box, thus addressing one of the limitations of direct interfacial simulations, namely slow diffusion through the interface. It is not clear, however, that this method is competitive in terms of accuracy with histogram-reweighting methods that can be used for the same models [28, 73].

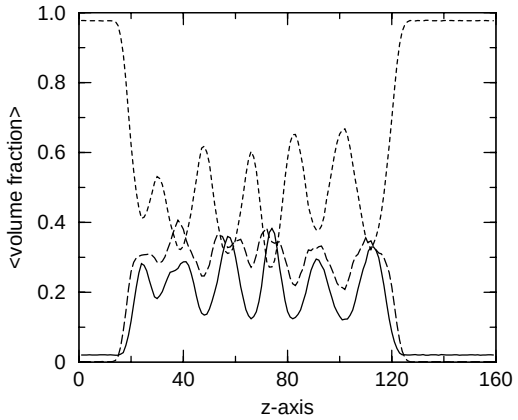

Figure 1. The volume fraction profile for a ternary oil–water–amphiphile system on a $20 \times 20 \times 160$ lattice. Continuous lines are for oil, long dashed lines for amphiphile and short dashed lines for water. Reprinted by permission from [22]. ©1996 American Institute of Physics.

3. Gibbs ensemble Monte Carlo simulation

The Gibbs ensemble Monte Carlo simulation methodology [29–31] enables direct simulations of phase equilibria in fluids. A schematic diagram of the technique is shown in figure 2. Let us consider a macroscopic system with two phases coexisting at equilibrium. Gibbs ensemble simulations are performed in two separate microscopic regions, each within periodic boundary conditions (denoted by the dashed lines in figure 2). The thermodynamic requirements for phase coexistence are that each region should be in internal equilibrium, and that temperature, pressure and the chemical potentials of all components should be the same in the two regions. System temperature in Monte Carlo simulations is specified in advance. The remaining three conditions are satisfied by performing three types of Monte Carlo move, displacements of particles within each region (to satisfy internal equilibrium), fluctuations in the volume of the

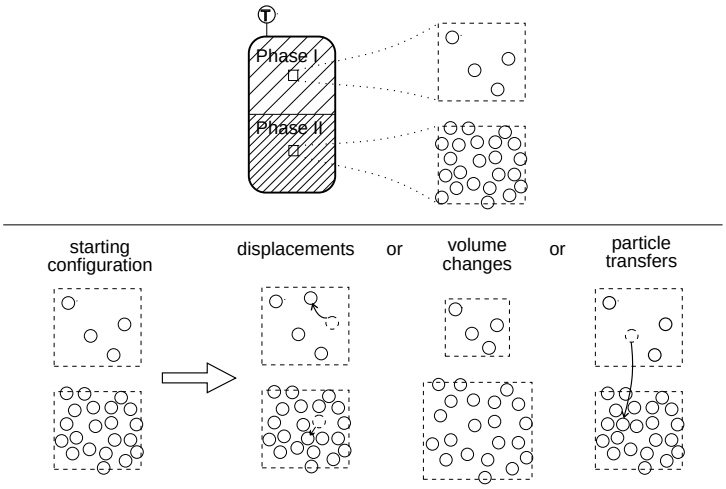

Figure 2. A schematic diagram of the Gibbs ensemble Monte Carlo simulation methodology.

two regions (to satisfy equality of pressures) and transfers of particles between regions (to satisfy equality of chemical potentials of all components).

The acceptance criteria for the Gibbs ensemble were originally derived from fluctuation theory [29]. An approximation was implicitly made in the derivation that resulted in a difference in the acceptance criterion for particle transfers proportional to $1/N$ relative to the exact expressions given subsequently [30]. A full development of the statistical mechanics of the ensemble was given by Smit *et al* [31] and Smit and Frenkel [32], which we follow here. A one-component system at constant temperature T, total volume V and total number of particles N is divided into two regions, with volumes V_I and $V_{II} = V - V_I$, and numbers of particles N_I and $N_{II} = N - N_I$. The partition function, Q_{NVT} is

$$Q_{NVT} = \frac{1}{\Lambda^{3N} N!} \sum_{N_I=0}^{N} \binom{N}{N_I} \int_0^V \mathrm{d}V_I \; V_I^{N_I} V_{II}^{N_{II}} \int \mathrm{d}\xi_I^{N_I} \; \exp[-\beta U_I(N_I)] \times \int \mathrm{d}\xi_{II}^{N_{II}} \; \exp[-\beta U_{II}(N_{II})] \tag{1}$$

where Λ is the thermal de Broglie wavelength, $\beta = 1/k_B T$, k_B is Boltzmann's constant, ξ_I and ξ_{II} are the scaled coordinates of the particles in the two regions and $U(N)$ is the total intermolecular potential of interaction of N particles. Equation (1) represents an ensemble with probability density $\wp(N_I, V_I; N, V, T)$:

$$\wp(N_I, V_I; N, V, T) \propto \frac{N!}{N_I! N_{II}!} \exp\left[N_I \ln V_I + N_{II} \ln V_{II} - \beta U_I(N_I) - \beta U_{II}(N_{II})\right]. \tag{2}$$

Smit *et al* [31] used the partition function given by equation (1) and a free-energy-minimization procedure to show that for a system with a first-order phase transition, the two regions in a Gibbs ensemble simulation are expected to reach the correct equilibrium densities.

The acceptance criteria for the three types of move can be immediately obtained from equation (2). For a displacement step internal to one of the regions, the probability of acceptance is the same as for conventional constant-NVT simulations:

$$\wp_{move} = \min[1, \exp(-\beta \, \Delta U)] \tag{3}$$

where ΔU is the configurational energy change resulting from the displacement. For a volume change step during which the volume of region I is increased by ΔV with a corresponding decrease of the volume of region II,

$$\wp_{volume} = \min\left[1, \exp\left(- \beta \, \Delta U_I - \beta \, \Delta U_{II} + N_I \ln \frac{V_I + \Delta V}{V_I} + N_{II} \ln \frac{V_{II} - \Delta V}{V_{II}} \right)\right]. \tag{4}$$

Equation (4) implies that sampling is performed uniformly in the volume itself. The acceptance criterion for particle transfers, written here for transfer from region II to region I, is

$$\wp_{transfer} = \min\left[1, \frac{N_{II} V_I}{(N_I + 1) V_{II}} \exp(-\beta \, \Delta U_I - \beta \, \Delta U_{II})\right]. \tag{5}$$

Equation (5) can be readily generalized to multicomponent systems. The only difference is that the number of particles of species j in each of the two regions, $N_{I,j}$ and $N_{II,j}$, replace N_I and N_{II} respectively. In simulations of multicomponent systems dilute in one component, it is possible that the number of particles of a species in one of the two regions becomes zero after a successful transfer out of that region. Equation (5) in this case is taken to imply that the probability of transfer out of an empty region is zero.

The acceptance rules to this point are for a simulation in which the total system is at constant number of molecules, temperature and volume. For pure component systems, the phase rule requires that only one intensive variable (in this case system temperature) can be

independently specified when two phases coexist. The vapour pressure is obtained from the simulation. By contrast, for multicomponent systems pressure can be specified in advance, with the total system being considered at constant NPT. The probability density for this case, $\wp(N_I, V_I; N, P, T)$, is

$$\wp(N_I, V_I; N, P, T) \propto \frac{N!}{N_I!N_{II}!} \exp\Big[N_I \ln V_I + N_{II} \ln V_{II} - \beta U_I(N_I) - \beta U_{II}(N_{II}) - \beta P(V_I + V_{II})\Big] \tag{6}$$

and the only change necessary in the algorithm is that the volume changes in the two regions are now made independently. The acceptance criterion for a volume change step in which the volume of region I is changed by ΔV, while the other region remains unchanged, is then

$$\wp_{volume} = \min\left[1, \exp\left(-\beta\,\Delta U_I + N_I \ln \frac{V_I + \Delta V}{V_I} - \beta P\,\Delta V\right)\right]. \tag{7}$$

An interesting extension of the original methodology was proposed by Lopes and Tildesley [33], to allow the study of more than two phases at equilibrium. The extension is based on setting up a simulation with as many boxes as the maximum number of phases expected to be present. Kristof and Liszi [34, 35] have proposed an implementation of the Gibbs ensemble in which the total enthalpy, pressure and number of particles in the total system are kept constant. Molecular dynamics versions of the Gibbs ensemble algorithm are also available [36–38].

The physical reason for the ability of the Gibbs ensemble to converge to a state that contains phases at their equilibrium density in the corresponding boxes, rather than a mixture of the two phases in each box, is the free-energy cost for creating and maintaining an interface. Essentially, in the Gibbs ensemble, one trades off the directness of the interfacial simulation approach with the (slight) inconvenience of setting up and maintaining two or more boxes for the equilibrium phases. However, much smaller system sizes can be used relative to interfacial simulations, and the simulations are generally stable, except in the immediate vicinity of critical points.

Near critical points Gibbs ensemble simulations become unstable because the free-energy penalty for creating an interface becomes small. In a detailed study of the behaviour of Gibbs ensemble simulations near critical points, Valleau [39] concluded that 'it is only with extreme care ... that reliable information on critical parameters or the shapes of coexistence curves may be obtained from Gibbs ensemble simulations.' The cause of the problems is that near critical points finite-size effects are present, and there is no mechanism for controlling system size of each individual region in the Gibbs ensemble. A better approach for dealing with systems near critical points is provided by the histogram methods described in section 5. The finite-size critical behaviour of the Gibbs ensemble has been examined by Bruce [40], Mon and Binder [41] and Panagiotopoulos [42]. The 'standard' procedure for obtaining critical points from Gibbs ensemble simulations is to fit subcritical coexistence data to universal scaling laws. This approach has a weak theoretical foundation, since the universal scaling laws are only guaranteed to be valid in the immediate vicinity of the critical point, where simulations give the wrong (classical) behaviour due to the truncation of the correlation length at the edge of the simulation box. In many cases, however, the resulting critical points are in reasonable agreement with more accurate results obtained from finite-size scaling methods (section 5.3).

In summary, the Gibbs ensemble Monte Carlo methodology provides a direct and efficient route to the phase coexistence properties of fluids, for calculations of moderate accuracy. The method has become a standard tool for the simulation community, as evidenced by the large

number of applications using the method that are described in section 7. Histogram-reweighting techniques (section 5) have the potential for higher accuracy, especially if equilibria at a large number of state points are to be determined. Histogram methods are also inherently better at determining critical points. In its original form, the Gibbs ensemble method is not practical for multisegment or strongly interacting systems, but development of configurational-bias sampling methods described in section 6.1 has overcome this limitation.

4. The NPT + test particle method, Gibbs–Duhem integration and pseudo-ensembles

4.1. The NPT + test particle method

The NPT + test particle method [43, 44] is based on calculations of the chemical potentials for a number of state points. A phase coexistence point is determined at the intersection of the vapour and liquid branches of the chemical potential versus pressure diagram. The Widom test particle method [14] or any other suitable method [15] can be used to obtain the chemical potentials. Corrections to the chemical potential of the liquid and vapour phases can be made, using standard thermodynamic relationships, for deviations between the pressure at which the calculations were made and the actual coexistence pressure. Extrapolations with respect to temperature are also possible [45].

In contrast to the Gibbs ensemble case, a number of simulations are required per coexistence point, but the number can be quite small, especially for vapour–liquid equilibrium calculations away from the critical point. For example, for a one-component system near the triple point, the density of the dense liquid can be obtained from a single NPT simulation at zero pressure. The chemical potential of the liquid, in turn, determines the density of the (near-ideal) vapour phase, so only one simulation is required. The method has been extended to mixtures [46, 47]. Significantly lower statistical uncertainties were obtained in [47] compared to earlier Gibbs ensemble calculations of the same Lennard-Jones binary mixtures, but the NPT + test particle method calculations were based on longer simulations.

The NPT + test particle method shares many characteristics with the histogram-reweighting methods discussed in section 5. In particular, histogram-reweighting methods also obtain the chemical potentials and pressures of the coexisting phase from a series of simulations. The corrections to the chemical potentials for changes in pressure [44] and temperature [45] are similar to the concept of reweighting of combined histograms from grand canonical simulations to new densities and temperatures.

Spyriouni *et al* [48, 49] have presented a powerful method (called 'SPECS') for calculations of polymer phase behaviour related to the NPT + test particle method. The method of Spyriouni *et al* targets the calculation of the phase behaviour of long-chain systems for which the test particle method for calculation of chemical potentials fails. For sufficiently long chains, even the configurational-bias sampling methods discussed in section 6.1 become impractical. For binary mixtures of a low-molecular-weight solvent (species 1) and a polymer (species 2), two parallel simulations are performed in the (μ_1, N_2, P, T) ensemble at conditions near the expected coexistence curve. The chemical potential of component 2 is determined through the 'chain increment' technique [50]. Iterative calculations at corrected values of the chemical potential of the solvent are performed until the chemical potential of the polymer in the two phases is equal. For the special case of a dilute solutions, estimates of the chemical potentials of the solvent and polymer for compositions different from the original simulation conditions can be made using standard thermodynamic relations and the number of required iterations is significantly reduced.

4.2. Gibbs–Duhem integration

Most methods for determination of phase equilibria by simulation rely on particle insertions to equilibrate or determine the chemical potentials of the components. Methods that rely on insertions experience severe difficulties for dense or highly structured phases. If a point on the coexistence curve is known (e.g. from Gibbs ensemble simulations), the remarkable method of Kofke [51, 52] enables the calculation of a complete phase diagram from a series of constant-pressure simulations that do not involve any transfers of particles. For one-component systems, the method is based on integration of the Clausius–Clapeyron equation over temperature:

$$\left(\frac{\mathrm{d}P}{\mathrm{d}\beta}\right)_{sat} = -\frac{\Delta H}{\beta\,\Delta V} \tag{8}$$

where sat indicates that the equation holds on the saturation line, and ΔH is the difference in enthalpy between the two coexisting phases. The right-hand side of equation (8) involves only 'mechanical' quantities that can be simply determined in the course of a standard Monte Carlo or molecular dynamics simulation. From the known point on the coexistence curve, a change in temperature is chosen, and the saturation temperature at the new temperature is predicted from equation (8). Two independent simulations for the corresponding phases are performed at the new temperature, with gradual changes of the pressure as the simulations proceed to take into account the enthalpies and densities at the new temperature as they are being calculated.

Questions related to propagation of errors and numerical stability of the method have been addressed in [52] and [53]. Errors in initial conditions resulting from uncertainties in the coexistence densities can propagate and increase with distance from the starting point when the integration path is towards the critical point [53]. Near critical points, the method suffers from instability of a different nature. Because of the small free-energy barrier for conversion of one phase into the other, even if the coexistence pressure is set properly, the identity of each phase is hard to maintain and large fluctuations in density are likely. The solution to this last problem is to borrow an idea from the Gibbs ensemble method and couple the volume changes of the two regions [52]. Extensions of the method to calculations of three-phase coexistence lines are presented in [54] and to multicomponent systems in [53]. Unfortunately, for multicomponent systems the Gibbs–Duhem integration method cannot avoid particle transfers—however, it avoids transfers for one component, typically the one that is the hardest to transfer. The method and its applications have been recently reviewed [55].

In some cases, in particular lattice and polymeric systems, volume change moves may be hard to perform, but particle insertions and deletions may be relatively easy, especially when using configurational-bias methods. Escobedo and de Pablo [58, 59] proposed a modification of the Gibbs–Duhem approach that is based on the expression

$$\left(\frac{\mathrm{d}(\beta\mu)}{\mathrm{d}\beta}\right)_{sat} = -\frac{\Delta(\rho u)}{\Delta\rho} \tag{9}$$

where ρ is the density $(=N/V)$ and u the energy per particle. This method was applied to continuous-phase polymeric systems in [58] and to lattice models in [60].

The Gibbs–Duhem integration method excels in calculations of solid–fluid coexistence [56, 57], for which other methods described in this paper are not applicable. An extension of the method that assumes that the initial free-energy difference between the two phases is known in advance, rather than requiring it to be zero, has been proposed by Meijer and El Azhar [61]. The procedure has been used in [61] to determine the coexistence lines of a hard-core Yukawa model for charge-stabilized colloids.

4.3. Pseudo-ensembles

The Gibbs–Duhem integration method represents a successful combination of numerical methods and molecular simulations. Taking this concept even further, Mehta and Kofke [62] proposed a 'pseudo-grand canonical ensemble' method in which a system maintains a constant number of particles and temperature, but has a fluctuating volume to ensure that, at the final density, the imposed value of the chemical potential is matched. The formalism still requires that estimates of the chemical potential be made during the simulation. The main advantage of the approach over more traditional grand canonical ensemble methods is that it provides additional flexibility with respect to the method to be used for determination of the chemical potential. For example, the 'chain increment' method [50] for chain molecules, which cannot be combined with grand canonical simulations, can be used for the chemical potential evaluations in a pseudo-grand canonical simulation (as in [48]).

The same 'pseudo-ensemble' concept has been used by Camp and Allen [63] to obtain a 'pseudo-Gibbs' method in which particle transfers are substituted for with volume fluctuations of the two phases. The volume fluctuations are unrelated to the ones required for pressure equality (equation (4)) but are instead designed to correct imbalances in the chemical potentials of some of the components detected, for example, by test particle particle insertions.

While the main driving force in [62] and [63] was to avoid direct particle transfers, Escobedo and de Pablo [59] designed a 'pseudo-NPT' method to avoid direct volume fluctuations which may be inefficient for polymeric systems, especially on lattices. Escobedo [64] extended the concept for bubble-point and dew-point calculations in a 'pseudo-Gibbs' method and proposed extensions of the Gibbs–Duhem integration techniques for tracing coexistence lines in multicomponent systems [65].

5. Histogram-reweighting grand canonical Monte Carlo simulation

Early in the history of development of simulation methods it was realized that a single calculation can, in principle, be used to obtain information on the properties of a system for a range of state conditions [66–68]. However, the practical application of this concept was severely limited by the performance of computers available at the time. In more recent years, several groups have confirmed the usefulness of this concept, first in the context of simulations of spin systems [69–71] and later for continuous-space fluids [72–76]. In the following subsections, we give a pedagogical review of histogram-reweighting methods for grand canonical Monte Carlo (GCMC) simulations as applied to one- and multicomponent systems. In addition, determinations of critical parameters from histogram data are briefly reviewed.

5.1. One-component systems

A GCMC simulation for a one-component system is performed as follows. The simulation cell has a fixed volume V, and is placed under periodic boundary conditions. The inverse temperature, $\beta = 1/k_BT$, and the chemical potential, μ, are specified as input parameters to the simulation. Histogram reweighting requires collection of data for the probability $f(N, E)$ of occurrence of N particles in the simulation cell with total configurational energy in the vicinity of E. This probability distribution function follows the relationship

$$f(N, E) = \frac{\Omega(N, V, E)\exp(-\beta E + \beta\mu N)}{\Xi(\mu, V, \beta)} \tag{10}$$

where $\Omega(N, V, E)$ is the microcanonical partition function (density of states) and $\Xi(\mu, V, \beta)$ is the grand partition function. Neither Ω nor Ξ are known at this stage, but Ξ is a constant for a run at given conditions. Since the left-hand side of equation (10) can be easily measured in a simulation, an estimate for Ω and its corresponding thermodynamic function, the entropy $S(N, V, E)$, can be obtained by a simple transformation of equation (10):

$$S(N, V, E)/k_B = \ln \Omega(N, V, E) = \ln f(N, E) + \beta E - \beta\mu N + C. \tag{11}$$

C is a run-specific constant. Equation (11) is meaningful only over the range of densities and energies covered in a simulation. If two runs at different chemical potentials and temperatures have a region of overlap in the space of (N, E) sampled, then the entropy functions can be 'merged' by requiring that the functions are identical in the region of overlap. To illustrate this concept, we make a one-dimensional projection of equation (10) to obtain

$$f(N) = \frac{Q(N, V, \beta) \exp(\beta\mu N)}{\Xi(\mu, V, \beta)}. \tag{12}$$

Histograms for two runs at different chemical potentials are presented in figure 3. There is a range of N over which the two runs overlap. Figure 4 shows the function $\ln f(N) - \beta\mu N$ for the data of figure 3. From elementary statistical mechanics, this function is related to the Helmholtz energy:

$$\beta A(N, V, \beta) = -\ln Q(N, V, \beta) = \ln f(N) - \beta\mu N + C. \tag{13}$$

Figure 4 shows the raw curves for μ_1 and μ_2 as well as a 'composite' curve formed by shifting data for the two runs by the amount indicated by the arrows. The combined curve provides information over the combined range of particle numbers, N, covered by the two runs. Note that by keeping only one-dimensional histograms for N we are restricted to combining runs at the same temperature, while the more general form (equation (11)) allows combination of runs at different temperatures.

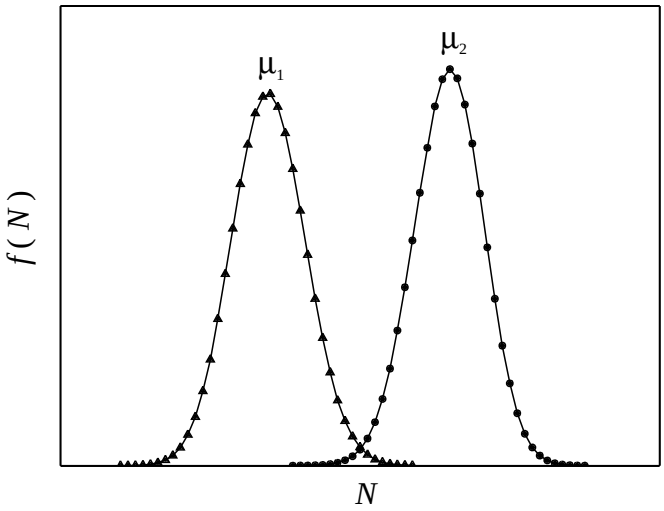

Figure 3. A schematic diagram of the probability $f(N)$ of occurrence of N particles for two GCMC runs for a pure component system at the same volume V and temperature T, but different chemical potentials, μ_1 and μ_2.

Simulation data are subject to statistical (sampling) uncertainties, which are particularly pronounced near the extremes of particle numbers and energies visited during a run. When data

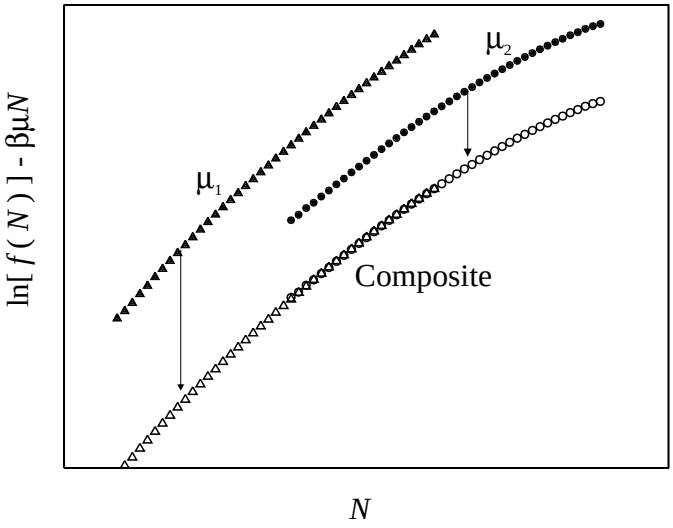

Figure 4. The function $\ln[f(N)] - \beta\mu N$ for the data of figure 3. The figure shows the raw curves for μ_1 and μ_2 as well as a 'composite' curve formed by shifting the data by the amount indicated by the arrows.

from multiple runs are combined as shown in figure 4, the question arises of how to determine the optimal amount by which to shift the raw data in order to obtain a global free-energy function. Ferrenberg and Swendsen [77] provided a solution to this problem by minimizing the differences between predicted and observed histograms. In this approach, it is assumed that multiple overlapping runs, $i = 1, 2, \ldots, R$, are available for a given system. The composite probability, $\wp(N, E; \mu, \beta)$, of observing N particles and energy E, if one takes into account all runs and assumes that they have the same statistical efficiency, is

$$\wp(N, E; \mu, \beta) = \left(\sum_{i=1}^{R} f_i(N, E) \exp[-\beta E + \beta\mu N]\right) \Big/ \left(\sum_{i=1}^{R} K_i \exp[-\beta_i E + \beta_i \mu_i N - C_i]\right) \tag{14}$$

where K_i is the total number of observations ($K_i = \sum_{N,E} f_i(N, E)$) for run i. The constants C_i (also known as 'weights') are obtained by iteration from the relationship

$$\exp(C_i) = \sum_{E} \sum_{N} \wp(N, E; \mu_i, \beta_i). \tag{15}$$

Given an initial guess for the set of weights C_i, equations (14) and (15) can be iterated until convergence is achieved. When many histograms are to be combined, this convergence of the Ferrenberg–Swendsen weights can take a long time. Once this has been achieved, however, all thermodynamic quantities for the system over the range of densities and energies covered by the histograms can be obtained. For example, the mean configurational energy $U(\mu, \beta)$ is

$$\langle U \rangle_{\mu,\beta} = \sum_{E} \sum_{N} \wp(N, E; \mu, \beta) E \tag{16}$$

and the mean density $\rho(\mu, \beta)$ is

$$\langle \rho \rangle_{\mu,\beta} = \frac{1}{V} \sum_{E} \sum_{N} \wp(N, E; \mu, \beta) N. \tag{17}$$

The pressure of a system can be obtained from the following expression. If the conditions for run 1 are (μ_1, V, β_1) and for run 2 (μ_2, V, β_2), then

$$C_2 - C_1 = \ln \frac{\Xi(\mu_2, V, \beta_2)}{\Xi(\mu_1, V, \beta_1)} = \beta_2 P_2 V - \beta_1 P_1 V \tag{18}$$

where P is the pressure, since $\ln \Xi = \beta P V$. Equation (18) can be used to obtain the absolute value of the pressure for one of the two runs, provided that the absolute pressure can be estimated for the other run. Typically, this is done by performing simulations for low-density states for which the system follows the ideal-gas equation of state, $PV = Nk_BT$.

Up to this point, we assumed that a system exists in a one-phase region over the range of densities and energies sampled. If a phase transition exists, then the system, *in principle*, should sample states on either side of the phase transition, resulting in histograms with multiple peaks. This is illustrated in figure 5, in which actual simulation data (from a single run) are plotted for a simple-cubic-lattice homopolymer system [73] at a slightly subcritical temperature. There are two states sampled by the run, one at low and one at high particle numbers, corresponding to the gas and liquid states. The conditions for phase coexistence are equality of temperature, chemical potential and pressure—the first two are satisfied by construction. From equation (18), the integral under the probability distribution function is proportional to the pressure. In the case of two distinct phases, the integrals should be calculated separately under the liquid and gas peaks. The condition of equality of pressures can be satisfied by reweighting the data until this condition is met. In section 5.3, we discuss how near-critical histogram data can be used to obtain precise estimates of the critical parameters for a transition.

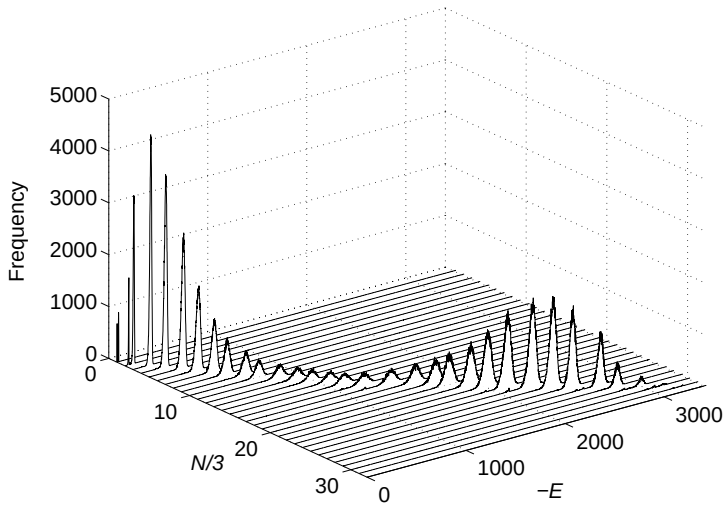

Figure 5. Frequency of observation of states versus energy, E, and number of particles, N, for a homopolymer of chain length $r = 8$ and coordination number $z = 6$ on a $10 \times 10 \times 10$ simple cubic lattice. The conditions, following the notation of [73], are $T^* = 11.5$, $\mu^* = -60.4$. In order to reduce clutter, data are plotted only for every third particle.

In the absence of phase transitions or at temperatures near a critical point, the values of all observable quantities (such as the histograms of energy and density) are independent of initial conditions, since free-energy barriers for transitions between states are small or non-existent. However, at lower temperatures, free-energy barriers for nucleation of new phases become increasingly large. The states sampled at a given temperature and chemical potential depend on initial conditions, a phenomenon known as hysteresis. This is illustrated

schematically in figure 6. For a supercritical isotherm, $T > T_c$, the mean value of the density is a continuous function of the chemical potential, and the same value is obtained for given conditions, irrespective of the starting configuration. By contrast, for a subcritical isotherm, when the runs are started from a low-density state, at some value of the chemical potential, a discontinuous 'jump' to a state of higher density is observed. The exact location of the jump depends on the initial state and the specific mix of Monte Carlo moves used to change the configuration of the system. When simulations are started in a high-density state, the system remains on the high-density branch of the isotherm until some value of the chemical potential is reached that is lower than the chemical potential of the jump from low- to high-density states.

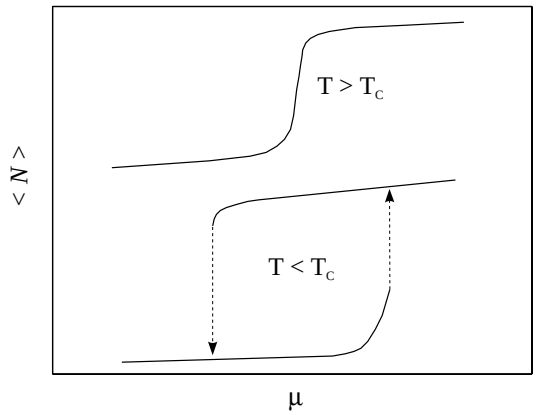

Figure 6. A schematic diagram of the mean number of particles, $\langle N \rangle$, versus the chemical potential, μ, for a subcritical and a supercritical isotherm of a one-component fluid. The curve for the supercritical isotherm has been shifted up for clarity.

The histogram-reweighting method can be applied to systems with large free-energy barriers for transitions between states, provided that care is taken to link all states of interest via reversible paths. One possibility is to utilize umbrella or multicanonical sampling techniques [71, 78] to artificially enhance the frequency with which a simulation samples the intermediate-density region [72]. Multicanonical and umbrella sampling require as input an estimate of the free energy in the intermediate-density region, which has to be obtained by trial and error. In addition, a significant fraction of simulation time is spent sampling unphysical configurations of intermediate density. An alternative approach is to link states by providing connections through a supercritical path, in a process analogous to thermodynamic integration [5]. This approach is illustrated schematically in figure 7. The filled square represents the critical point for a transition, and open squares linked by dashed lines represent tie lines. Ellipses represent the range of particle numbers and energies sampled by a single simulation. A near-critical simulation samples states on both sides of the coexistence curve, while subcritical simulations are likely to be trapped in (possibly metastable) states on either side. However, as long as there is a continuous path linking all states of interest, the free energies and pressures can be calculated correctly, and an accurate phase envelope can be obtained.

An example of the application of histogram reweighting for determining the phase behaviour of a homopolymer model on the simple cubic lattice is illustrated in figure 8. The phase behaviour and critical properties of the model for a range of chain lengths have been studied in [73]. The system in this example is for chain length $r = 8$ and coordination number $z = 6$. In this example, we first performed a simulation at reduced temperature $T^* = 11.5$

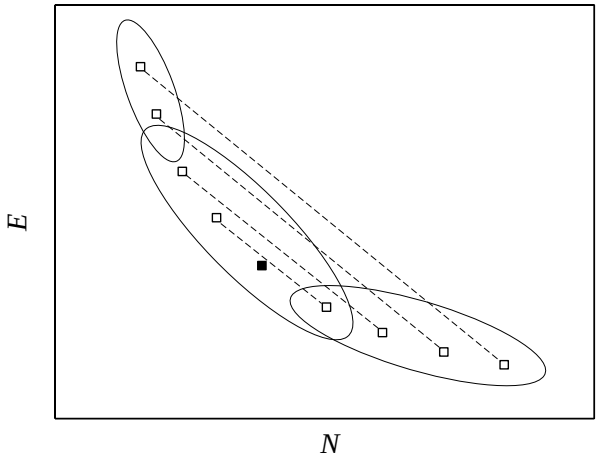

Figure 7. A schematic diagram of the energy, E, versus the number of particles, N, for a one-component fluid with a phase transition. Squares linked by dashed lines are coexisting phases joined by tie lines and the filled square indicates the critical point of the transition. Ellipses represent the range of particle numbers and energies sampled during different GCMC runs.

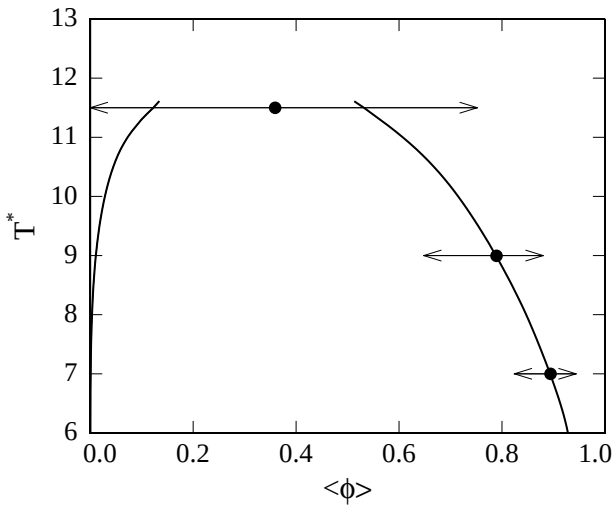

Figure 8. A phase diagram for a homopolymer of chain length $r = 8$ on a $10 \times 10 \times 10$ simple cubic lattice of coordination number $z = 6$. Filled circles give the reduced temperature, T^*, and mean volume fraction, $\langle\phi\rangle$, of the three runs performed. Arrows from the run points indicate the range of densities sampled for each simulation. The thick continuous line is the estimated phase coexistence curve.

and chemical potential $\mu^* = -60.4$, for which the raw histogram data are shown in figure 5. The resulting average volume fraction for the run is indicated on figure 8 by the filled circle at $T^* = 11.5$. The range of volume fractions sampled during the simulation is indicated on figure 8 by the arrows originating at the run point. Because this run is near the critical point, a very broad range of particle numbers and thus volume fractions is sampled during this single run. The histogram from this run was then reweighted to lower temperatures and a preliminary phase diagram was obtained. The estimated coexistence chemical potential at $T^* = 9$ was

used as input to a new simulation, which sampled states near the saturated liquid line. The same procedure was repeated, now with combined histograms from the first two runs, to obtain an estimate of the coexistence chemical potential at $T^* = 7$. A new simulation was performed to sample the properties of the liquid at that temperature. The total time for the three runs was 10 CPU min on a Pentium III 300 MHz processor. The final result of these three calculations was the phase coexistence lines shown by the thick continuous lines in figure 8.

Two general observations can be made in relation to this example. First, it should be pointed out that the histogram-reweighting method works much faster on smaller system sizes. As system size increases, relative fluctuations in the number of particles and energy for a single run at specified conditions decrease as the $1/2$ power of the system volume V. This implies that more simulations are required to obtain overlapping histograms that cover the range of energies and densities of interest. Moreover, the number of Monte Carlo moves required to sample properties increases approximately linearly with system size in order to keep the number of moves per particle constant. The computational cost of each Monte Carlo move is proportional to system size for pairwise-additive long-range interactions and independent of system size for short-range interactions. The net effect is that the total computational effort required to obtain a phase diagram at a given accuracy scales as the 1.5 to 2.5 power of system volume, respectively, for short- and long-range interactions. Fortunately, away from critical points, the effect of system size on the location of the coexistence curves for first-order transitions is typically small. In this example, calculations on a 15^3 system result in phase coexistence lines practically indistinguishable from the ones shown in figure 8. The mean absolute relative differences for the coexistence densities between the small and large systems are 0.1% for the liquid and 1% for the (much-lower-density) gas, well within the width of the coexistence lines in figure 8.

A second observation relates to calculations near critical points. The coexistence lines in figure 8 do not extend above a temperature of $T^* = 11.6$ because above that temperature significant overlap exists between the liquid and vapour peaks of the histograms. This overlap renders calculations of the liquid and gas densities imprecise. Larger system sizes suffer less from this effect and can be used to obtain coexistence densities near critical points. As discussed in section 5.3, a sequence of studies with increasing system size are also required to obtain accurate estimates of critical points.

5.2. Multicomponent systems

The histogram-reweighting methodology for multicomponent systems [74–76] closely follows the one-component version described above. The probability distribution function for observing N_1 particles of component 1 and N_2 particles of component 2 with configurational energy in the vicinity of E for a GCMC simulation at imposed chemical potentials μ_1 and μ_2, respectively, at inverse temperature β in a box of volume V is

$$f(N_1, N_2, E) = \frac{\Omega(N_1, N_2, V, E)\exp(-\beta E + \beta\mu_1 N_1 + \beta\mu_2 N_2)}{\Xi(\mu_1, \mu_2, V, \beta)}. \tag{19}$$

Equations (11) to (18) can be similarly extended to multicomponent systems.

The main complication in the case of multicomponent systems relative to the one-component case is that the dimensionality of the histograms is one plus the number of components, thus making their machine storage and manipulation somewhat more challenging. For example, in the case of one-component systems, it is possible to store the histograms directly as two-dimensional arrays. The memory requirements for storing three-dimensional arrays for a two-component system make it impractical to do so. Instead, lists of observations of particle numbers and energies are periodically stored on disk. It is important to select

the frequency of sampling of the histogram information so that only essentially independent configurations are sampled. This implies that sampling is done less frequently at high densities for which the acceptance ration of the insertion and removal steps is lower. Sampling essentially independent configurations also enforces the condition of equal statistical efficiency underlying the Ferrenberg–Swendsen histogram combination equations (14) and (15).

5.3. Critical point determination

Recent advances in the determination of critical parameters for fluids lacking special symmetries have been based on the concept of mixed-field finite-size scaling and have been reviewed in detail by Wilding [79]. As a critical point is approached, the correlation length ξ grows without bound and eventually exceeds the linear system size L of the simulation box. Singularities and discontinuities that characterize critical behaviour in the thermodynamic limit are smeared out and shifted in finite systems. The infinite-volume critical point of a system can, however, be extracted by examining the size dependence of thermodynamic observables, through finite-size scaling theory [80–82]. The finite-size scaling approach proposed by Bruce and Wilding [83, 84] accounts for the lack of symmetry between coexisting phases in most continuous-space fluids. For one-component systems, the ordering operator, M, is proportional to a linear combination of the number of particles N and total configurational energy U:

$$M \propto N - sU \tag{20}$$

where s is the field-mixing parameter. For multicomponent systems, an extra field-mixing parameter appears for each added component—for example for binary systems,

$$M \propto N_1 - sU - qN_2 \tag{21}$$

where q is the field-mixing parameter for the number of particles of component 2.

General finite-size scaling arguments predict that the normalized probability distribution for the ordering operator M at criticality, $\wp(M)$, has a universal form. The order parameter distribution for the three-dimensional Ising universality class is shown in figure 9 as a continuous line. Also shown in figure 9 are data for a homopolymer of chain length $r = 200$ on a $50 \times 50 \times 50$ simple cubic lattice of coordination number $z = 26$ [73]. The data were obtained by histogram-reweighting methods, by adjusting the chemical potential, temperature and field-mixing parameter s so as to obtain the best possible fit to the universal distribution. The non-universal constant A and the critical value of the ordering operator M_c were chosen so that the data have zero mean and unit variance. Due to finite-size corrections to scaling, the apparent critical temperature, $T_c(L)$, and density, $\rho_c(L)$, deviate from their infinite-system values, $T_c(\infty)$ and $\rho_c(\infty)$. They are expected to follow scaling relationships with respect to the simulated system size, L:

$$\begin{aligned} T_c(L) - T_c(\infty) &\propto L^{-(\theta+1)/\nu} \\ \rho_c(L) - \rho_c(\infty) &\propto L^{-(1-\alpha)/\nu} \end{aligned} \tag{22}$$

where θ, ν and α are, respectively, the correction-to-scaling exponent, the correlation length exponent and the exponent associated with the heat capacity divergence. For the three-dimensional Ising universality class, the approximate values of these exponents are [85, 86] $(\theta, \nu, \alpha) \approx (0.54, 0.629, 0.11)$. Figure 10 demonstrates these scaling relationships for the critical temperature and density of the square-well fluid of range $\lambda = 3$ [87].

5.4. Thermodynamic and Hamiltonian scaling

Finally in this section, we would like to mention briefly two methods that are related to histogram reweighting. Thermodynamic scaling techniques proposed by Valleau [88] are

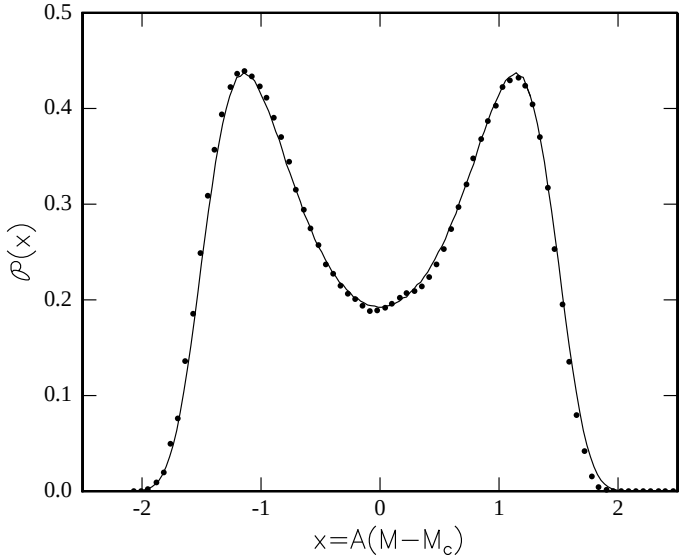

Figure 9. The ordering operator distribution for the three-dimensional Ising universality class (continuous line—data courtesy of N B Wilding). Points are for a homopolymer of chain length $r = 200$ on a $50 \times 50 \times 50$ simple cubic lattice of coordination number $z = 26$ [73]. The non-universal constant A and the critical value of the ordering operator M_c were chosen so that the data have zero mean and unit variance.

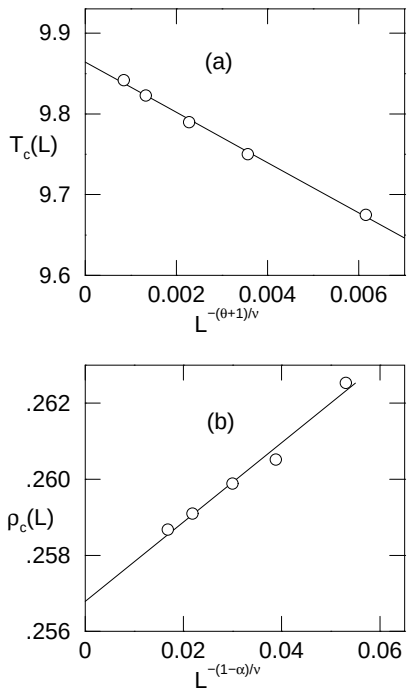

Figure 10. Critical temperature (a) and density (b) scaling with linear system size for the square fluid of range $\lambda = 3$. Solid lines represent a least-squares fit to the points. Reprinted by permission from [87]. ©1999 American Institute of Physics.

based on calculations in the NPT rather than the grand canonical (μVT) ensemble and provide information for the free energy over a range of volumes rather than a range of particle numbers. Thermodynamic scaling techniques can also be designed to cover a range of Hamiltonians (potential models) in the Gibbs [89] or grand canonical [90] ensembles. In their Hamiltonian scaling form, the methods are particularly useful for optimizing parameters in intermolecular potential models to reproduce experimental data such as the coexisting densities and vapour pressures. Thermodynamic and Hamiltonian scaling methods require estimates for the free energy of the system as a function of the conditions, so that the system can be forced to sample the range of states of interest with roughly uniform probability, as for the umbrella sampling Monte Carlo method [78].

6. Smart sampling for difficult systems

6.1. Configurational-bias sampling

The most common bottleneck in achieving convergence in methods that rely on particle transfers is the prohibitively low acceptance of transfer attempts. For dense fluid phases, especially for complex, orientation-dependent intermolecular potentials, configurations with 'holes' in which an extra particle can be accommodated are highly improbable, and the converse step of removing a particle involves a large cost in energy. Configurational-bias sampling techniques significantly improve sampling efficiency for Gibbs or grand canonical Monte Carlo simulations. The methods have been reviewed in detail in [5, 13] and the chapter by Frenkel in [10] and will only be covered briefly in the present article.

Configurational-bias methods trace their ancestry to biased sampling for lattice polymer configurations proposed by Rosenbluth and Rosenbluth [91]. Development of configurational-bias methods for canonical and grand canonical simulations and for continuous-space models took place in the early 1990s [92–96] and dramatically expanded the range of intermolecular potential models that can be studied by the methods described in the previous sections.

Configurational-bias methods are based on segment-by-segment insertions or removals of a multisegment molecule. Several trial directions are attempted for every segment insertion, and a favourable growth direction is preferentially selected for the segment addition. In this way, the acceptance probability of insertions is greatly enhanced. For each segment growth or removal step, a correction factor (often called 'Rosenbluth weight') is calculated. The product of the Rosenbluth weights of all steps is incorporated in the overall acceptance criterion for particle insertions and removals in order to correct for the bias introduced by the non-random growth along preferential directions.

6.2. Expanded ensembles

Another approach for handling multisegment molecules is based on the concept of expanded ensembles [97–100]. Expanded ensembles for chain molecules construct a series of intermediate states for the molecule of interest, from a non-interacting (phantom) chain to the actual chain with all segments and interactions in place. These intermediate states can be semi-penetrable chains of the full length [97, 98] or shortened versions of the actual chain [99, 100]. Estimates of the free energy of the intermediate states are required to ensure roughly uniform sampling, as for thermodynamic and Hamiltonian scaling methods mentioned in the previous section. The advantage of expanded ensembles over configurational-bias methods is that arbitrarily complex long molecules can be sampled adequately, if sufficient computational effort is invested in constructing good approximations of the free energies of intermediate states.

7. Applications

The methods described in the previous sections enable fast and accurate calculations of the phase behaviour of fluids. Their availability has resulted in a veritable explosion in the number of studies of the phase behaviour of both simple 'toy model' and realistic potentials for fluids in the past decade. Previous reviews [6–9] have covered applications of such methods up to 1995, so the focus of the following sections will be on research that has been published since 1995.

The section is divided into three subsections. In the first, we discuss studies of model systems, such as the square well of Lennard-Jones fluids, that do not aim at representing exactly a given real fluid. Studies of the phase behaviour of model systems are made for testing theoretical models of the phase behaviour and elucidating general characteristics of the phase behaviour due to 'generic' interactions present in broad classes of systems. The last two subsections are devoted to studies of realistic models of pure fluids and mixtures, respectively. The primary purpose of these studies is to obtain quantitative agreement with experimental data.

7.1. Model systems

Simple spherically symmetric model potentials have been the subject of several studies over the period covered in the present review. Square-well fluids with ranges $\lambda = 1.5$ and 3 were studied by histogram methods in [101] and fluids with $\lambda = 2$ in [102], using Gibbs ensemble calculations. The critical point of the full Lennard-Jones (6, 12) pure fluid was obtained by histogram methods first under hyperspherical boundary conditions [103] and later under conventional periodic boundary conditions [76]. The estimate from the critical point from this last study is $T_c^* = 1.313\,20 \pm 0.000\,07$, $\rho_c^* = 0.316 \pm 0.001$. Gas–liquid nucleation for the Lennard-Jones system was studied by [104]. The phase diagram of the hard-core Yukawa fluid with parameters adjusted to mimic the Lennard-Jones fluids was obtained in [105]. Exponential-6 fluids were studied by [106] and [90]. The effect of three-body Axilrod–Teller interactions on vapour–liquid and liquid–liquid equilbria was studied in [107, 108]. Spherically symmetric model potentials with varying interaction range have been studied by [110–112], in order to model protein precipitation and crystallization. A combination of Gibbs ensemble calculations for the liquid–solid parts of the phase diagrams and Gibbs–Duhem integration for the liquid–solid parts were used in these studies. As the range of the attractive interactions is decreased, it is found that the liquid–solid critical point becomes metastable because solidification occurs first.

Binary Lennard-Jones mixtures were studied by [113], using the multiple-box extension of the Gibbs ensemble method [33]. Closed-loop immiscibility behaviour was found for this system that has only isotropic interactions using a set of parameters with cross-interaction diameter with a negative deviation from the Lorentz–Berthelot rule. Liquid–vapour phase behaviour of a symmetric binary Lennard-Jones fluid mixture was studied by Wilding *et al* [75] using histogram methods. Depending on the relative strength of the unlike-pair interactions, the phase diagram was found to include a tricritical point. The phase behaviour of the Widom–Rowlinson mixture was studied in [114]. The Widom–Rowlinson mixture is a two-component fluid where like species do not interact and unlike species interact via a hard-core repulsion. As the density is increased this fluid phase separates. Phase separation in binary mixtures of hard spheres with non-additive diameters was studied in [115]. Phase equilibria for model ternary chain systems were studied by [22, 116, 117]. A mixture of square-well particles with directional bonding interactions was studied by Davies *et al* [118]. The system has a closed

immiscibility loop, with miscibility at low temperatures being promoted by association between unlike components. Vapour–liquid equilibria for a monomer–dimer square-well mixture were also obtained by the same group [119, 120].

Several studies of model one-component systems with non-spherical interactions have been published. Polydisperse systems of infinitely thin platelets have been studied by means of semi-grand Gibbs simulations by [121]. Segregation of the larger particles in the nematic phase was observed. The same group [122] studied the phase behaviour of rodlike colloids with attractive interactions. The effect of attractive interactions on the phase behaviour of the Gay–Berne liquid-crystal model has been studied in [123]. Phase equilibria in long-chain lattice polymer models were studied by [19, 28, 73].

Studies of polar fluids included pure and mixed dipolar fluids [124, 125], dipolar two-centre Lennard-Jones fluids [126], quasi-two-dimensional Stockmayer fluids [127], polarizable Stockmayer fluids [128] and quadrupolar fluids [129, 130]. Dipolar hard-core systems were found to exhibit an 'island' of vapour–liquid phase coexistence for a certain range of elongations [131]. A system with highly directional interactions was also found to lack normal vapour–liquid coexistence [132]. A central-force model potential for associating fluids was studied by [133] and homonuclear and heteronuclear Lennard-Jones chains with association sites were studied by [134].

The phase behaviour of the restricted primitive model was studied by histogram methods on the surface of a four-dimensional hypersphere [135, 136] and under normal periodic boundary conditions [87]. For this strongly interacting system, previous calculations using the Gibbs ensemble [101] were found to overestimate the true critical temperature of the model by 10%, due to apparent extensions of the coexistence curve to supercritical temperatures in finite systems. The same effects explain the overestimation of the critical temperature of the Lennard-Jones fluid from Gibbs ensemble studies discussed in the previous paragraph, even though the degree of overestimation is much lower for the less strongly interacting Lennard-Jones system.

7.2. Realistic potential models—pure fluids

A large number of intermolecular potential models for fluids are available (e.g. [137–141], optimized to reproduce the structural and energetic properties (heat of vaporization etc) of the liquid state around room temperature. Such models were not designed and cannot be expected to model accurately the phase coexistence properties, as demonstrated, for example, for *n*-alkanes [142, 143], water [144] and hydrogen fluoride [145, 146]. The simulation techniques for determining the phase behaviour described in previous sections of the present paper have only recently become able to handle complex, realistic potential models. A number of research groups are currently involved in the development of intermolecular potential models that can reproduce phase coexistence properties to near-experimental accuracy. Most of the models described in this section are effective two-body potentials, for reasons of computational expedience. The influence of three-body forces on the gas–liquid coexistence of argon was studied in [147].

Hydrocarbon molecules are ubiquitous in industrial processes and form the building blocks of biological systems. They are non-polar and consist of a small number of groups, thus making them the logical starting point for potential model development. Siepmann, Karaborni and Smit [142, 148, 149] used configurational-bias Gibbs ensemble simulations to obtain an optimized potential model and the critical properties of the *n*-alkanes homologous series. At the time, there were conflicting experimental data on the dependence of the critical density on chain length, which were resolved with the help of the simulations. Spyriouni *et al* [49] have studied the phase behaviour of *n*-hexadecane for the Dodd–Theodorou potential [150] and

obtained good agreement for the phase envelope but not for the vapour pressure. Branched alkanes have been studied by [151–154], perfluorinated alkanes by [155], fluoromethanes by [156, 157] and α-olephins by [158].

Three accurate united-atom potential sets for *n*-alkanes have appeared recently. The TRAPPE [159] and NERD models [160] use the Lennard-Jones (12,6) potential to describe non-bonded interactions among methyl and methylene groups, while the model of Errington and Panagiotopoulos [161] uses the exponential-6 functional form. All three reproduce the experimental phase diagrams and critical points. The exponential-6 model is slightly better as regards representation of the vapour pressures. Figures 11 and 12 illustrate the quality of representation of experimental data for the newer optimized models. Deviations from experimental data for the exponential-6 united atom model are comparable to those for a recently developed explicit hydrogen model [162].

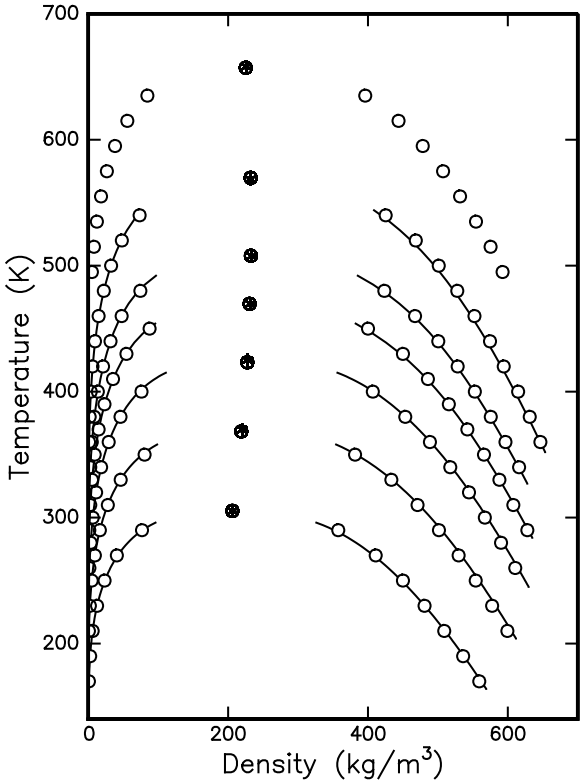

Figure 11. Phase diagrams of select *n*-alkanes. The curves from bottom to top are for ethane, propane, butane, pentane, hexane, octane and dodecane. Circles represent calculations for the model of [161]. Uncertainties are smaller than the size of the symbols. A solid line is used for experimental data and an asterisk for the experimental critical point. Reprinted by permission from [161]. ©1999 American Chemical Society.

The phase behaviour of C_{60} has been investigated [109, 163–165] using spherically symmetric potentials in order to determine whether the system lacks a liquid phase. Model systems with sufficiently short range attractive interactions do not have a stable liquid phase because the liquid–solid transition pre-empts the normal liquid–vapour transition, as mentioned in section 7.1. The answer for C_{60} is unclear; some studies [109, 164] report a narrow liquid region, while others [163,165] suggest that the liquid–vapour critical point lies in the metastable

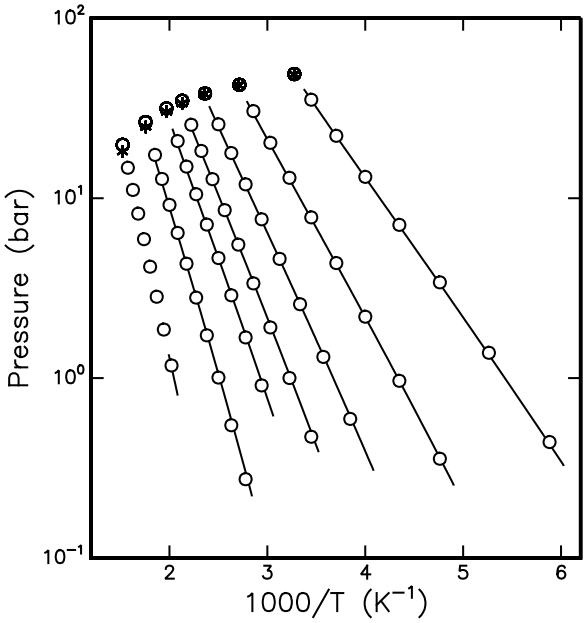

Figure 12. Vapour pressures of selected *n*-alkanes. The curves from right to left are for ethane, propane, butane, pentane, hexane, octane and dodecane. The symbols are the same as for figure 11. Reprinted by permission from [161]. ©1999 American Chemical Society.

region of the phase diagram.

Several studies of the phase behaviour of realistic models for polar fluids appeared in the period covered in the present review. The phase behaviour of alkanols was studied by [166], hydrogen sulphide was studied by [167], carbon disulphide by [168] and alkali fluids by [169]. Flexible models of water were studied by histogram methods by [170]. A modification of the SPCE model for water to better reproduce the vapour–liquid coexistence properties was proposed by [171]. Polarizable water models were studied by [172], who found rather disappointing agreement with experimental data for several literature polarizable potentials. A new fixed-point charge model for water based on the exponential-6 functional form for the non-polar interactions was proposed by [173]. The potential of [173] does an excellent job for the phase coexistence envelope and vapour pressure from the triple to the critical point of water, but fails to reproduce accurately the dielectric constant and structure of the liquid at room temperature.

Studies of the phase behaviour for some quantum fluids have appeared in recent years. Wang *et al* [174–176] studied the phase behaviour and free energy of H_2 and Ne at low temperatures using path integral versions of Gibbs and grand canonical Monte Carlo techniques that they developed. The same group later investigated the adsorption of hydrogen in graphitic slit pores [177].

7.3. Realistic potential models—mixtures

Alkane mixtures have been studied extensively in recent years. For example, Chen and Siepmann investigated supercritical ethane and *n*-heptane mixtures and obtained the free energy of transfer for *n*-pentane and *n*-heptane between He and *n*-heptane liquid phases [162]. Delhommelle *et al* [178] studied mixtures of *n*-alkanes using both a united-atom model [148]

and anisotropic united-atom models due to Toxvaerd [179, 180]. Other recent studies of alkane mixtures include [161, 181, 182]. The solubility of small molecules such N_2 and methane and their mixtures in polyethylene, including effects of polymer crystallinity, was studied in [183]. Mixtures with α-olephins were studied in [48, 158]. In general, excellent agreement between experiment and simulation results is obtained for these non-polar mixtures, provided that the pure component potentials have been optimized to reproduce the phase envelope and vapour pressures of the pure components. No mixture parameters are necessary for the calculations.

Grand canonical histogram-reweighting Monte Carlo simulations were used to obtain the phase behaviour of several mixtures with polar and non-polar components in [182]. The conventional Lorentz–Berthelot combining rules [184], as well as a set of combining rules due to Kong [185], were used to obtain unlike-pair potential parameters. The Lorentz–Berthelot rules generally result in more attractive unlike-pair interactions than the Kong rules. For the *n*-alkane/CO_2 systems, predicted phase diagrams are in excellent agreement with experiment when the Kong combining rules are used but in significantly worse agreement when the Lorentz–Berthelot rules are used. An example is shown in figure 13 for the propane–CO_2 mixture. For mixtures with CH_3OH and H_2O, the Lorentz–Berthelot rules yield slightly better agreement with experiment than the Kong rules.

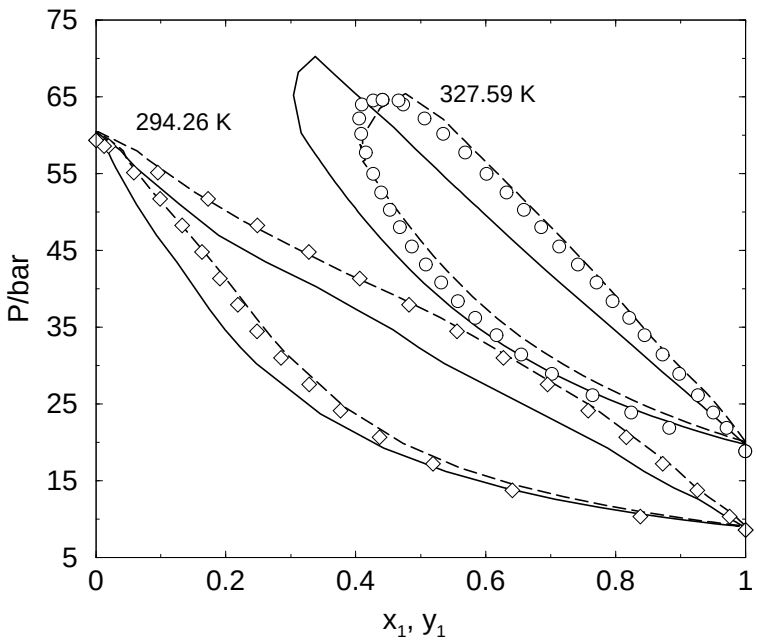

Figure 13. A propane/CO_2 pressure–composition diagram. Experimental data: $T = 327.59$ K (open circles) [193], $T = 294.26$ K (open diamonds) [194]. 1 bar $= 10^5$ Pa. GCMC simulations with the Lorentz–Berthelot (solid line) and Kong combining rules (dashed line). The average statistical uncertainties for the simulation data in pressure and composition are ± 0.47 bar and ± 0.0050, respectively. Reprinted by permission from [182]. ©1999 Taylor and Francis.

Other phase diagrams of realistic systems with polar components studied recently by simulation methods include those of methanol–ethane [186], methanethiol with propane [187], fluorocarbon mixtures [188] and mixtures of CO_2 with alkanes and fluoroalkanes [189]. The Lorentz–Berthelot rules were used in these studies. It is interesting that for the *n*-hexane–CO_2 mixture studied in [189] deviations of similar magnitude and direction to those for the

n-pentane–CO_2 were observed in [182] (continuous line in figure 13), even though different pure component potential models were used in the two studies. In other recent studies of binary and ternary systems with alkanes and CO_2 [190, 191], binary interaction parameters were used to acheive good agreement with experiment, a clearly less attractive alternative than *a priori* predictions based solely on pure component potentials. The Henry's law constants and phase diagrams for methane–water and ethane–water systems have been studied by [192], resulting in modest agreement with experimental data.

8. Concluding remarks

A novice researcher interested in obtaining the phase behaviour of a fluid is now faced with a bewildering choice among a number of alternative methods and their variations. In this section, similarities and differences among the methods, their relative performance and their ease of implementation will be discussed.

Simulations with an explicit interface appear, at first glance, to be relatively simple to implement and perform. Unlike most other methods discussed here, interfacial simulations can also be performed using molecular dynamics codes. However, they provide an inefficient route to the phase coexistence properties. Unless the properties of the interface itself (or the surface tension) are of interest, other methods discussed in the present article provide better alternatives.

The majority of recent studies discussed in section 7 have been performed using various implementations of the Gibbs ensemble, often combined with configurational-bias methods to improve sampling for multisegment molecules. The Gibbs method is relatively easy to implement and provides direct information on the properties of coexisting phases from a single simulation. One major weakness of the methodology is that it is not applicable to solid or highly structured phases. For such systems, the only possible choice is the Gibbs–Duhem integration method and its variations. The Gibbs–Duhem method, however, needs to start from a point on the coexistence curve.

The accuracy of the Gibbs ensemble method for a given amount of computer time does not seem to match the accuracy of histogram-reweighting methods [182]. Histogram-reweighting methods are also inherently better at determining critical points via the finite-size scaling formalism. On the negative side, the effort required to implement histogram combination and reweighting is more than for the Gibbs ensemble method. Histogram-reweighting methods are also indirect, requiring the assembly of the free-energy function of a system from a series of simulations. The efficiency of histogram methods decreases rapidly with system size. Despite these disadvantages, they are probably the most promising for future applications.

The NPT + test particle method shares with histogram-reweighting techniques the feature that it proceeds by computation of the chemical potential for a number of state points. Histogram-reweighting methods, however, cover a range of densities and temperatures in a single simulation. In addition, data from separate runs can be combined in a systematic way only for histogram-reweighting methods. A variation of the NPT + test particle method is the SPECS method for systems of long-chain molecules [48, 49]. The SPECS method is a good alternative to expanded-ensemble Gibbs Monte Carlo calculations for cases for which configurational-bias sampling methods become inefficient.

Interesting connections between many of the methods discussed in the present article have been pointed out by Escobedo [64, 65]. In particular, Escobedo suggests that Gibbs–Duhem integration, pseudo-ensembles and the NPT + test particle method can be considered as low-order approximations of a histogram-reweighting approach.

In the area of applications, an important goal for research in the coming years will be to

develop a set of pure component group-based potentials and combining rules that can be used for general predictions of both pure component and mixture phase behaviour. Early results for realistic mixtures [182] suggest that relatively simple intermolecular potential models can be used to predict the phase behaviour of broad classes of binary systems. For mixtures with large differences in polar character of the components, however, present models do not always result in quantitative agreement with experiment. New models that include higher-order interactions such as polarizability may be suitable for this purpose, a hypothesis that will need to be tested in the future.

Acknowledgments

Research in the author's group on which this article is based was supported by the Department of Energy (Office of Basic Energy Sciences), the National Science Foundation, the American Chemical Society Petroleum Research Fund and the Camille and Henry Dreyfus Foundation.

References

[1] Rowlinson J S and Swinton F S 1982 *Liquids and Liquid Mixtures* 3rd edn (London: Butterworth Scientific)
[2] Prausnitz J M, Lichtenthaler R N and de Azevedo E G 1999 *Molecular Thermodynamics of Fluid Phase Equilibria* 3rd edn (New York: Prentice-Hall)
[3] Hansen J-P and Verlet L 1969 *Phys. Rev.* **184** 151–61
[4] Allen M P and Tildesley D J 1987 *Computer Simulation of Liquids* (Oxford: Oxford University Press)
[5] Frenkel D and Smit B 1996 *Understanding Molecular Simulation* (London: Academic)
[6] Panagiotopoulos A Z 1992 *Mol. Simul.* **9** 1–23
[7] Smit B 1993 *Computer Simulations in Chemical Physics (NATO ASI Series C, vol 397)* ed M P Allen and D J Tildesley (Dordrecht: Kluwer) pp 173–209
[8] Panagiotopoulos A Z 1994 *Supercritical Fluids, Fundamentals for Applications (NATO ASI Series E, vol 273)* ed E Kiran and J M H Levelt Sengers (Dordrecht: Kluwer) pp 411–37
[9] Panagiotopoulos A Z 1995 *Observation, Prediction and Simulation of Phase Transitions in Complex Fluids (NATO ASI Series C, vol 460)* ed M Baus, L F Rull and J-P Ryckaert (Dordrecht: Kluwer) pp 463–501
[10] Baus M, Rull L F and Ryckaert J-P (ed) 1995 *Observation, Prediction and Simulation of Phase Transitions in Complex Fluids (NATO ASI Series C, vol 460)* (Dordrecht: Kluwer)
[11] Binder K 1997 *Rep. Prog. Phys.* **60** 487–559
[12] Deem M W 1998 *AIChE J.* **44** 2569–96
[13] Siepmann J I 1999 *Monte Carlo Methods Chem. Phys.* **105** 443–60
[14] Widom B 1963 *J. Chem. Phys.* **39** 2808–12
[15] Kofke D A and Cummings P T 1997 *Mol. Phys.* **92** 973–96
[16] Rowlinson J S and Widom B 1982 *Molecular Theory of Capillarity* (Oxford: Clarendon) ch 6
[17] Gubbins K E 1989 *Mol. Simul.* **2** 223–52
[18] Holcomb C, Clancy P and Zollweg J 1993 *Mol. Phys.* **78** 437–59
[19] Yan Q, Liu H and Hu Y 1996 *Macromolecules* **29** 4066–71
[20] Madden W G, Pesci A I and Freed K F 1990 *Macromolecules* **23** 1181–91
[21] Mackie A D, Panagiotopoulos A Z and Kumar S K 1995 *J. Chem. Phys.* **102** 1014–23
[22] Mackie A, Onur K and Panagiotopoulos A Z 1996 *J. Chem. Phys.* **104** 3718–25
[23] Harris J G 1992 *J. Phys. Chem.* **96** 5077–86
[24] Hariharan A and Harris J G 1994 *J. Chem. Phys.* **101** 4156–65
[25] Alejandre J, Tildesley D J and Chapela G A 1995 *J. Chem. Phys.* **102** 4574–83
[26] Mecke M, Winkelmann J and Fischer J 1997 *J. Chem. Phys.* **107** 9264–70
[27] Diaz-Herrera E, Alejandre J, Ramirez-Santiago G and Forstmann F 1999 *J. Chem. Phys.* **110** 8084–9
[28] Frauenkron H and Grassberger P 1997 *J. Chem. Phys.* **107** 9599–608
[29] Panagiotopoulos A Z 1987 *Mol. Phys.* **61** 813–26
[30] Panagiotopoulos A Z, Quirke N, Stapleton M and Tildesley D J 1988 *Mol. Phys.* **63** 527–45
[31] Smit B, De Smedt P and Frenkel D 1989 *Mol. Phys.* **68** 931–50
[32] Smit B and Frenkel D 1989 *Mol. Phys.* **68** 951–8
[33] Lopes J N C and Tildesley D J 1997 *Mol. Phys.* **92** 187–95

[34] Kristof T and Liszi J 1997 *Mol. Phys.* **90** 1031–4
[35] Kristof T and Liszi J 1998 *Mol. Phys.* **94** 519–25
[36] Hentschke R *et al* 1996 *J. Mol. Modell.* **2** 319–26
[37] Kotelyanskii M J and Hentschke R 1996 *Mol. Simul.* **17** 95–112
[38] Baranyai A and Cummings P T 1996 *Mol. Simul.* **17** 21–5
[39] Valleau J P 1998 *J. Chem. Phys.* **108** 2962–6
[40] Bruce A D 1997 *Phys. Rev.* E **55** 2315–20
[41] Mon K K and Binder K 1992 *J. Chem. Phys.* **96** 6989–95
[42] Panagiotopoulos A Z 1989 *Int. J. Thermophys.* **10** 447–57
[43] Möller D and Fischer J 1990 *Mol. Phys.* **69** 463–73
Möller D and Fischer J 1990 *Mol. Phys.* **75** 1461–2 (erratum)
[44] Lotfi A, Vrabec J and Fischer J 1992 *Mol. Phys.* **76** 1319–33
[45] Boda D, Liszi J and Szalai I 1995 *Chem. Phys. Lett.* **235** 140–5
[46] Vrabec J and Fischer J 1995 *Mol. Phys.* **85** 781–92
[47] Vrabec J, Lotfi A and Fischer J 1995 *Fluid Phase Equil.* **112** 173–97
[48] Spyriouni T, Economou I G and Theodorou D N 1998 *Phys. Rev. Lett.* **80** 4466–9
[49] Spyriouni T, Economou I G and Theodorou D N 1998 *Macromolecules* **31** 1430–1
[50] Kumar S K, Szleifer I and Panagiotopoulos A Z 1991 *Phys. Rev. Lett.* **66** 2935–8
[51] Kofke D A 1993 *Mol. Phys.* **78** 1331–6
[52] Kofke D A 1993 *J. Chem. Phys.* **98** 4149–62
[53] Mehta M and Kofke D A 1994 *Chem. Eng. Sci.* **49** 2633–45
[54] Agrawal R, Mehta M and Kofke D A 1994 *Int. J. Thermophys.* **15** 1073–83
[55] Kofke D A 1999 *Adv. Chem. Phys.* **105** 405–41
[56] Agrawal R and Kofke D A 1995 *Phys. Rev. Lett.* **74** 122–5
[57] Bolhuis P and Frenkel D 1997 *J. Chem. Phys.* **106** 666–87
[58] Escobedo F A and de Pablo J J 1997 *J. Chem. Phys.* **106** 9858–68
[59] Escobedo F A and de Pablo J J 1997 *J. Chem. Phys.* **106** 2911–23
[60] Escobedo F A and de Pablo J J 1997 *Europhys. Lett.* **40** 111–17
[61] Meijer E J and El Azhar F 1997 *J. Chem. Phys.* **106** 4678–83
[62] Mehta M and Kofke D A 1995 *Mol. Phys.* **86** 139–47
[63] Camp P J and Allen M P 1996 *Mol. Phys.* **88** 1459–69
[64] Escobedo F A 1998 *J. Chem. Phys.* **108** 8761–72
[65] Escobedo F A 1999 *J. Chem. Phys.* **110** 11 999–2010
[66] McDonald I R and Singer K 1967 *J. Chem. Phys.* **47** 4766–72
[67] Wood W W 1968 *J. Chem. Phys.* **48** 415–34
[68] Card D N and Valleau J P 1970 *J. Chem. Phys.* **52** 6232–40
[69] Bennett C H 1976 *J. Comput. Phys.* **22** 245–68
[70] Ferrenberg A M and Swendsen R H 1988 *Phys. Rev. Lett.* **61** 2635–8
[71] Berg B A and Neuhaus T 1992 *Phys. Rev. Lett.* **68** 9–12
[72] Wilding N B 1995 *Phys. Rev.* E **52** 602–11
[73] Panagiotopoulos A Z, Wong V and Floriano M A 1998 *Macromolecules* **31** 912–18
[74] Wilding N B 1997 *Phys. Rev.* E **55** 6624–31
[75] Wilding N B, Schmid F and Nielaba P 1998 *Phys. Rev.* E **58** 2201–12
[76] Potoff J J and Panagiotopoulos A Z 1998 *J. Chem. Phys.* **109** 10 914–20
[77] Ferrenberg A M and Swendsen R H 1989 *Phys. Rev. Lett.* **63** 1195–8
[78] Torrie G M and Valleau J P 1977 *J. Comput. Phys.* **23** 187–99
[79] Wilding N B 1997 *J. Phys.: Condens. Matter* **9** 585–612
[80] Ferdinand A E and Fisher M E 1969 *Phys. Rev.* **185** 832–46
[81] Fisher M E and Barber M N 1972 *Phys. Rev. Lett.* **28** 1516–19
[82] Privman V (ed) 1990 *Finite Size Scaling and Numerical Simulation of Statistical Mechanical Systems* (Singapore: World Scientific)
[83] Bruce A D and Wilding N B 1992 *Phys. Rev. Lett.* **68** 193–6
[84] Wilding N B and Bruce A D 1992 *J. Phys.: Condens. Matter* **4** 3087–108
[85] Sengers J V and Levelt-Sengers J N H 1986 *Annu. Rev. Phys. Chem.* **37** 187–222
[86] Liu A J and Fisher M E 1989 *Physica* A **156** 35–76
[87] Orkoulas G and Panagiotopoulos A Z 1999 *J. Chem. Phys.* **110** 1581–90
[88] Valleau J P 1999 *Monte Carlo Methods Chem. Phys.* **105** 369–404
[89] Kiyohara K *et al* 1996 *Mol. Phys.* **89** 965–74

[90] Errington J R and Panagiotopoulos A Z 1998 *J. Chem. Phys.* **109** 1093–100
[91] Rosenbluth M N and Rosenbluth A W 1955 *J. Chem. Phys.* **23** 356–9
[92] Frenkel D, Mooij G C A M and Smit B 1992 *J. Phys.: Condens. Matter* **4** 3053–76
[93] de Pablo J J, Laso M, Siepmann J I and Suter U W 1993 *Mol. Phys.* **80** 55–63
[94] Siepmann J I and McDonald I R 1993 *Mol. Phys.* **79** 457–73
[95] Mooij G C A M, Frenkel D and Smit B 1992 *J. Phys.: Condens. Matter* **4** L255–9
[96] Laso M, de Pablo J J and Suter U W 1992 *J. Chem. Phys.* **97** 2817–19
[97] Lyubartsev A, Martsinovski A and Shevkunov S 1992 *J. Chem. Phys.* **96** 1776–83
[98] Vorontsov-Velyaminov P, Broukhno A and Kuznetsova T 1996 *J. Phys. Chem.* **100** 1153–8
[99] Wilding N B and Müller M 1994 *J. Chem. Phys.* **101** 4324–30
[100] Escobedo F and de Pablo J J 1996 *J. Chem. Phys.* **105** 4391–4
[101] Orkoulas G and Panagiotopoulos A Z 1994 *J. Chem. Phys.* **101** 1452–9
[102] de Miguel E 1997 *Phys. Rev.* E **55** 1347–54
[103] Caillol J M 1998 *J. Chem. Phys.* **109** 4885–93
[104] Ten Wolde P R and Frenkel D 1998 *J. Chem. Phys.* **109** 9901–18
[105] Kalyuzhnyi Y V and Cummings P T 1996 *Mol. Phys.* **87** 1459–62
[106] Tavares F W and Sandler S I 1996 *Mol. Phys.* **87** 1471–6
[107] Sadus R J 1998 *Fluid Phase Equil.* **144** 351–9
[108] Sadus R J 1998 *Fluid Phase Equil.* **151** 63–72
[109] Caccamo C, Costa D and Fucile A 1997 *J. Chem. Phys.* **106** 255–63
[110] Hagen M H J and Frenkel D 1994 *J. Chem. Phys.* **101** 4093–7
[111] Ten Wolde P R and Frenkel D 1997 *Science* **277** 1975–7
[112] Tavares F W and Sandler S I 1997 *AIChE J.* **43** 218–31
[113] Lopes J N C 1999 *Mol. Phys.* **96** 1649–58
[114] Shew C Y and Yethiraj A 1996 *J. Chem. Phys.* **104** 7665–70
[115] Dijkstra M 1998 *Phys. Rev.* E **58** 7523–8
[116] Jiang J, Yan Q, Liu H and Hu Y 1997 *Macromolecules* **30** 8459–62
[117] de Miguel E and da Gama M M T 1997 *J. Chem. Phys.* **107** 6366–78
[118] Davies L A, Jackson G and Rull L F 1999 *Phys. Rev. Lett.* **82** 5285–8
[119] McCabe G, Gil-Villegas A and Jackson G 1999 *Chem. Phys. Lett.* **303** 27–36
[120] Davies L A *et al* 1999 *Phys. Rev.* E **57** 2035–44
[121] Bates M A and Frenkel D 1999 *J. Chem. Phys.* **110** 6553–9
[122] Bolhuis P G, Stroobants A, Frenkel D and Lekkerkerker H N W 1997 *J. Chem. Phys.* **107** 1551–64
[123] de Miguel E *et al* 1996 *J. Chem. Phys.* **105** 4234–49
[124] Sadus R J 1996 *Mol. Phys.* **87** 979–90
[125] Sadus R J 1996 *Mol. Phys.* **89** 1187–94
[126] Lisal M, Budinsky R and Vacek V 1997 *Fluid Phase Equil.* **135** 193–207
[127] Gao G T, Zeng X C and Wang W C 1997 *J. Chem. Phys.* **106** 3311–7
[128] Kiyohara K, Gubbins K E and Panagiotopoulos A Z 1997 *J. Chem. Phys.* **106** 3338–47
[129] O'Shea S F, Dubey G S and Rasaiah J C 1997 *J. Chem. Phys.* **107** 237–42
[130] Vega C *et al* 1998 *J. Mol. Liq.* **76** 157–69
[131] McGrother S C and Jackson G 1996 *Phys. Rev. Lett.* **76** 4183–6
[132] Blair M J and Patey G N 1998 *Phys. Rev.* E **57** 5682–6
[133] Bresme F, Lomb E and Abascal J L F 1997 *J. Chem. Phys.* **106** 1569–75
[134] Blas F J and Vega L F 1997 *Mol. Phys.* **92** 135–50
[135] Caillol J M, Levesque D and Weis J J 1996 *Phys. Rev. Lett.* **77** 4039–42
[136] Caillol J M, Levesque D and Weis J J 1997 *J. Chem. Phys.* **107** 1565–75
[137] Jorgensen W L, Madura J D and Swenson C J 1984 *J. Am. Chem. Soc.* **106** 6638–46
[138] Cornell W D *et al* 1995 *J. Am. Chem. Soc.* **117** 5179–97
[139] Halgren T A 1996 *J. Comput. Chem.* **17** 490–615
[140] Smith J C and Karplus M 1992 *J. Am. Chem. Soc.* **114** 801–12
[141] Jorgensen W L, Maxwell D S and Tirado-Rives J 1996 *J. Am. Chem. Soc.* **118** 11 225–36
[142] Siepmann J I, Karaborni S and Smit B 1993 *J. Am. Chem. Soc.* **115** 6454–5
[143] Chen B, Martin M G and Siepmann I G 1998 *J. Phys. Chem.* B **102** 2578–86
[144] Errington J R and Panagiotopoulos A Z 1998 *J. Phys. Chem.* B **102** 7470–5
[145] Visco D P and Kofke D A 1999 *Fluid Phase Equil.* **160** 37–47
[146] Visco D P and Kofke D A 1998 *J. Chem. Phys.* **109** 4015–27
[147] Anta J A, Lomba E and Lombardero M 1997 *Phys. Rev.* E **55** 2707–12

[148] Smit B, Karaborni S and Siepmann J I 1995 *J. Chem. Phys.* **102** 2126–40
[149] Siepmann J I, Karaborni S and Smit B 1993 *Nature* **365** 330–2
[150] Dodd L R and Theodorou D N 1994 *Adv. Polym. Sci.* **116** 249–81
[151] Cui S T, Cummings P T and Cochran H D 1997 *Fluid Phase Equil.* **141** 45–61
[152] Siepmann J I, Martin M G, Mundy C J and Klein M L 1997 *Mol. Phys.* **90** 687–93
[153] Martin M G and Siepmann J I 1999 *J. Phys. Chem.* B **103** 4508–17
[154] Zhuravlev N D and Siepmann J I 1997 *Fluid Phase Equil.* **134** 55–61
[155] Cui S T, Siepmann J I, Cochran H D and Cummings P T 1998 *Fluid Phase Equil.* **146** 51–61
[156] Potter S C *et al* 1997 *Mol. Phys.* **92** 825–33
[157] Jedlovszky P and Mezei M 1999 *J. Chem. Phys.* **110** 2991–3002
[158] Spyriouni T, Economou I G and Theodorou D N 1999 *J. Am. Chem. Soc.* **121** 3407–13
[159] Martin M G and Siepmann J I 1998 *J. Phys. Chem.* B **102** 2569–77
[160] Nath S K, Escobedo F A and de Pablo J J 1998 *J. Chem. Phys.* **108** 9905–11
[161] Errington J R and Panagiotopoulos A Z 1999 *J. Phys. Chem.* B **103** 6314–22
[162] Chen B and Siepmann J I 1999 *J. Phys. Chem.* B **103** 5370–9
[163] Hagen M H J, Meijer E J, Mooij G C A M and Frenkel D 1993 *Nature* **365** 425–6
[164] Cheng A, Klein M L and Caccamo C 1993 *Phys. Rev. Lett.* **71** 1200–3
[165] Hasegawa M and Ohno K 1997 *J. Phys.: Condens. Matter* **9** 3361–70
[166] Van Leeuwen M E 1996 *Mol. Phys.* **87** 87–101
[167] Kristof T and Liszi J 1997 *J. Phys. Chem.* B **101** 5480–3
[168] Kristof T, Liszi J and Szalai I 1996 *Mol. Phys.* **89** 931–42
[169] Velasco E *et al* 1996 *J. Non-Cryst. Solids* Part 2 **207** 897–900
[170] Conrad P B and de Pablo J J 1998 *Fluid Phase Equil.* **150** 51–9
[171] Boulougouris G C, Economou I G and Theodorou D N 1998 *J. Phys. Chem.* B **102** 1029–35
[172] Kiyohara K, Gubbins K E and Panagiotopoulos A Z 1988 *Mol. Phys.* **94** 803–8
[173] Errington J R and Panagiotopoulos A Z 1998 *J. Phys. Chem.* B **102** 7470–5
[174] Wang Q U, Johnson J K and Broughton J Q 1997 *Mol. Phys.* **89** 1105–19
[175] Wang Q Y and Johnson J K 1997 *Fluid Phase Equil.* **132** 93–116
[176] Wang Q Y, Johnson J K and Broughton J Q 1997 *J. Chem. Phys.* **107** 5108–17
[177] Wang Q Y and Johnson J K 1998 *Int. J. Thermophys.* **19** 835–44
[178] Delhommelle J, Boutin A, Tavitian B, Mackie A D and Fuchs A H 1999 *Mol. Phys.* **96** 1517–24
[179] Padilla P and Toxvaerd S 1991 *J. Chem. Phys.* **95** 509–19
[180] Toxvaerd S 1997 *J. Chem. Phys.* **107** 5197–204
[181] Mackie A D, Tavitian B, Boutin A and Fuchs A H 1997 *Mol. Simul.* **19** 1–15
[182] Potoff J J, Errington J R and Panagiotopoulos A Z 1999 *Mol. Phys.* **97** 1073–83
[183] Nath S K and de Pablo J J 1999 *J. Phys. Chem.* B **103** 3539–44
[184] Maitland G C, Rigby M, Smith E B and Wakeham W A 1981 *Intermolecular Forces* (Oxford: Clarendon) pp 519–23
[185] Kong C L 1973 *J. Chem. Phys.* **59** 2464–7
[186] Gotlib I Y, Piotrovskaya E M and de Leeuw S W 1997 *Fluid Phase Equil.* **129** 1–13
[187] Agrawal R and Wallis E P 1997 *Fluid Phase Equil.* **131** 51–65
[188] Gao G T, Wang W C and Zeng X C 1999 *Fluid Phase Equil.* **160** 69–78
[189] Cui S T, Cochran H D and Cummings P T 1999 *J. Phys. Chem.* B **103** 4485–91
[190] Vrabec J and Fischer J 1997 *AIChE J.* **43** 212–7
[191] Liu A P and Beck T L 1998 *J. Phys. Chem.* B **102** 7627–31
[192] Errington J R *et al* 1998 *J. Phys. Chem.* B **102** 8865–73
[193] Niesen V G and Rainwater J C 1990 *J. Chem. Thermodyn.* **22** 777–88
[194] Reamer H H, Sage B H and Lacey W N 1951 *Indust. Eng. Chem.* **43** 2515